J. Fluid Mech. (1977), *vol.* 82, *part* 4, *pp.* 705–723
Printed in Great Britain

Experiments on the structure of turbulence in fully developed pipe flow. Part 2. A statistical procedure for identifying 'bursts' in the wall layers and some characteristics of flow during bursting periods

By T. R. HEIDRICK, S. BANERJEE

Atomic Energy of Canada Limited, Whiteshell Nuclear Research Establishment, Pinawa, Manitoba, Canada

AND R. S. AZAD

Department of Mechanical Engineering, University of Manitoba, Winnipeg, Manitoba, Canada

(Received 1 December 1975 and in revised form 21 July 1976)

This paper is the second of a pair describing two-point velocity measurements in fully developed pipe flow. A method of processing hot-film anemometer signals to identify intervals of high energy production ('bursts') in wall turbulence is presented. The method uses filtered cross-stream spatial derivatives of the axial velocity fluctuations. It is demonstrated to be more sensitive to 'bursts' than several other methods of indentification. The bursts identified in this manner are shown to have similar characteristics to those observed in visual studies.

The technique has been applied to the wall region of turbulent pipe flow. Mean burst rates have been obtained at various distances from the wall for three Reynolds numbers. It is shown that the mean burst rate cannot be reliably obtained from a previously used technique based on the autocorrelation of the axial velocity fluctuations.

On the basis of our experiments, the mean burst rate and the turbulent shear stress have been found to vary similarly with distance from the wall. In the region near the wall where the shear stress is constant the mean burst rate is independent of the kinematic viscosity.

Some characteristics of the velocity fluctuations during burst intervals have been studied. All the bursts began with a relative minimum in the axial velocity fluctuations followed by a peak in the cross-stream spatial derivative. A second peak always occurred midway through the burst. The sequence of events is somewhat similar to that in the last stage of laminar-to-turbulent transition.

1. Introduction

In part 1 of this study (Heidrick, Banerjee & Azad 1977) we found that it is difficult to describe the turbulence structure near a wall in terms of a single average eddy or wave model. This is because two types of motion exist near a wall: (i) periods of intense activity and energy production separated by (ii) relatively quiescent periods. In this paper we present a sensitive method of identifying the interval of high energy production in the wall region by processing velocity measurements made with

hot-film anemometers. Some characteristics of the flow during these intervals are also discussed.

The visual studies of Kline *et al.* (1967) and Kim, Kline & Reynolds (1971) showed that longitudinal 'streaks' of slow- and fast-moving fluid exist side by side near the wall in a turbulent boundary layer. Intermittently, (i) the low-speed streaks lift away from the wall; (ii) the low-speed streaks develop into either transverse or streamwise vortices which migrate away from the wall and (iii) vortices break up into a more chaotic motion. This three-stage cycle was called 'bursting' or an active period.

Both the streaks (Richardson & Beatty 1959) and the periods of activity (Corino & Brodkey 1969) have also been observed in fully developed pipe flow. Corino & Brodkey photographed a small region near the wall using a camera moving with the flow. Their stages of bursting were called (i) deceleration, (ii) acceleration, (iii) ejection and (iv) sweep. This sequence began with a deceleration of a large portion of the flow near the wall. Faster-moving fluid then entered the field of view and began to cause the slower fluid to accelerate. This was followed by an ejection of fluid from the slower region. The sequence was completed when the field of view was swept clean of the slower fluid.

In simple geometries these visual techniques can be used to identify 'bursts'. However, it is difficult to determine statistics related to the velocities (such as the energy spectrum) from visual studies alone. Thus our first objective was to develop a method of processing anemometer signals to identify bursts so that quantitative measurements of the turbulence structure could be made during these intervals. Offen & Kline (1975) have performed a simultaneous visual/hot-film anemometer study of a turbulent boundary layer in parallel with our work. They investigated the relationship between visual observations and several methods of conditionally sampling the hot-film signal to detect bursts. They also concluded that at present there is no really adequate detection scheme.

Although the importance of bursts has been demonstrated (both Kim, Kline & Reynolds (1968) and Wallace, Eckelmann & Brodkey (1972) have shown that most of the production of turbulence occurs during bursts), their cause remains unknown. Our second objective was to study the flow during bursts in more detail and to obtain information regarding mechanisms that cause bursts.

In the next section, previous attempts to identify bursts from hot-film anemometer signals are reviewed. A brief description of the experimental facility and procedures is given in §3; our burst identification technique is then described and compared with visual studies. The results of applying this technique to fully developed pipe flow are presented and discussed in §4 and conclusions are presented in §5.

2. Previous methods of detecting bursts

Conditioned sampling methods of measuring the intermittent turbulent/non-turbulent regions in the outer structure of boundary layers have been investigated by both Kaplan & Laufer (1969) and Hedley & Keffer (1974). The major attempts to identify 'bursts' in the near-wall region by other than visual techniques have been by Kim *et al.* (1968) and Rao, Narasimha & Badri Narayanan (1971). Kim *et al.* hypothesized that the intermittent formation of low-speed streaks might appear as a near periodicity in the axial fluctuation velocity $u(t)$ near the wall. This was supported when they found a second peak in the autocorrelation of $u(t)$ at a time delay

equal to the average time interval $\bar{T}_B$ between bursts. However, this second peak was low and often disappeared when long averaging times were used. The technique could not pick out individual bursts for analysis.

Rao *et al.* (1971) devised a method for identifying bursts by processing hot-wire anemometer signals. They took the time derivative $\partial u(t)/\partial t$ of the axial velocity fluctuations and passed it through a narrow-band spectrum analyser centred at a high frequency in the turbulence spectrum. The output had intermittent periods of fluctuations with large amplitude. The average time between these periods agreed, when scaled, with the interval between bursts in the visual study of Kim *et al.* (1968). Rao *et al.* concluded that the visual bursts and the periods of large amplitude (or activity) in the output signal were caused by the same phenomenon. However, it was often difficult to discriminate between active and inactive periods and the experimenter had to exercise considerable judgement in identifying bursts.

In the experiments of Rao *et al.* (1971) two measurement parameters could affect the number of active periods: the filter centre-frequency and the amplitude level set to discriminate between active and quiescent periods. Although the number of active periods remained constant when these parameters were varied over particular narrow ranges, no method was found to predict *a priori* where these ranges were. Most of their results were obtained with a 'simple' counting procedure where these parameters were set on the basis of the experimenter's judgement. Also, two separate periods of large amplitude band-passed fluctuations were counted as a single burst if they were not separated by at least twice the period of the centre-frequency of the band-pass filter. This arbitrary rule also affects the measured number of bursts. Thus we felt that a more quantitative technique for identifying bursts was necessary and this led to the development of the technique described in this paper.

3. Experimental apparatus and procedures

3.1. *Experimental loop and velocity sensors*

The experiments were done in water ($\nu = 1{\cdot}022$ cS) in a 7·87 cm I.D. round tube. The characteristics of both the experimental loop and the test section have been discussed previously (Heidrick *et al.* 1977, referred to as part 1).

The hot-film probes used to measure the axial fluctuating velocities consisted of two sensors (0·051 mm in diameter, and 1·67 mm long with a 1 mm heated length) placed about 0·254 mm apart in the orientations shown in figure 1. The sensor separations were measured using an optical comparitor and were 0·254 mm, 0·3048 mm and 0·2032 mm for configurations 1, 2 and 3 respectively. Unless stated otherwise, the results presented are based on configuration 1. Sensor characteristics and operating procedures were discussed in part 1.

3.2. *Signal processing and data acquisition*

A description is given in part 1 of how the anemometer signals from the two velocity sensors were recorded on analog tape. The d.c. component in each signal was removed by high-pass filtering. The sensitivities of the signals were then equalized and at this stage each signal essentially represented the fluctuating velocity. A spatial velocity difference was formed as shown schematically in figure 2. This velocity difference

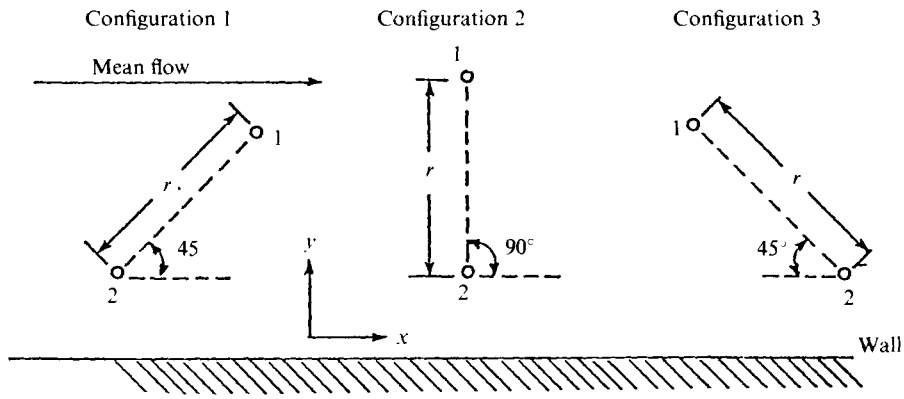

FIGURE 1. Configurations of the two sensor probes used.

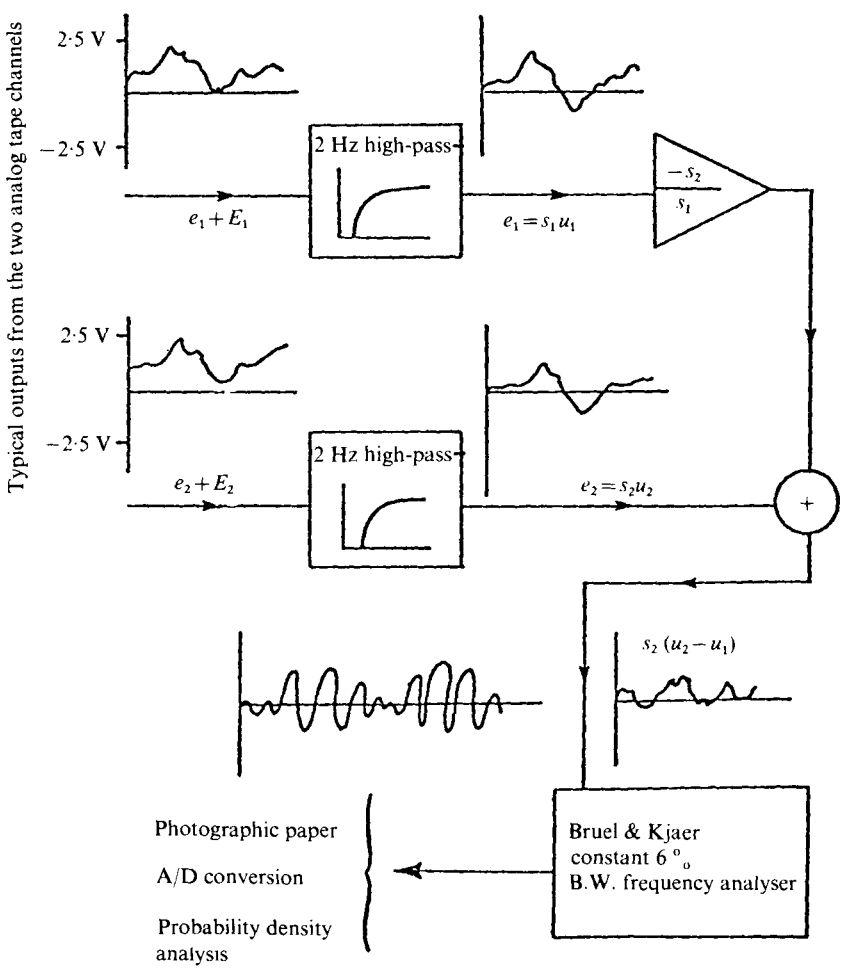

FIGURE 2. Signal processing schematic.

signal was passed through a Bruel & Kjaer Model 2107 spectrum analyser (6% bandwidth) whose output was either recorded by an oscillograph, fed into an amplitude probability density analyser or digitized simultaneously with the fluctuating velocity signals.

The simultaneous analog-to-digital conversion of the narrow-band-passed velocity difference and each of the fluctuating velocity signals was done under the control of an external clock with the A/D conversion facility described in detail by Saltvold (1971). The data were continuously stored on digital magnetic tape at a sampling rate of 2000 samples/s for each A/D converter channel. One minute records were used.

3.3. *Burst identification technique*

The technique devised to identify bursts and the relationship between measured and visually observed bursts are described in this subsection.

The method. Previous visual studies have indicated two main phenomena associated with bursts. These are rapid acceleration of the flow field and the development of inflexions in the velocity profile. A spatial derivative formed by differencing the signals from the sensors in configuration 1 (see figure 1) is sensitive to both these phenomena. We therefore examined this spatial derivative to determine whether it would lead to a method for identifying bursts.

Figure 3(*a*) shows a typical axial velocity trace. The unprocessed signal did not show anything that could be defined as a burst. Passing this signal through a spectrum analyser† set high in the spectrum (figure 3*b*) showed some intermittent periods of high activity but the bursts were buried in background noise. Comparison of figures 3(*b*) and (*c*) shows that this situation was only marginally improved by taking the time derivative of the signal before filtering. This was the procedure adopted by Rao *et al.* and in our opinion it is difficult to identify the bursts unambiguously. However, use of the filtered spatial derivative of the velocity as shown in figure 3(*d*) makes the bursts stand out much more clearly. The spatial derivative gave the clearest separation between active and quiescent periods. The extent of this discrimination between active and quiescent periods is estimated later by a 'flatness' factor. Band-pass filtering was necessary to make the bursts stand out. The unfiltered time and spatial derivatives are shown later (figure 11). They do not indicate the periods when bursts occur.

Determination of mean burst rates. In figure 4 we show that, while the amplitude of the signal during bursts changes the background level, the bursts retain their identity over a range of filter centre-frequencies. The calculated burst rate is therefore independent of the centre-frequency f_c over this range. But the record that most clearly distinguishes active from quiescent periods ('on' from 'off') is the one with the highest ratio of burst to background level. For an 'on–off' process of this type, this is the record that has the maximum flatness factor. For the signals shown in figure 4, the maximum flatness factor occurs for filter centre-frequencies between 125 and 135 Hz. The filter centre-frequency which gives the maximum flatness factor results in the best discrimination and is considered the optimum setting.

If the amplitude of the optimally filtered signal is larger than a preset discriminator

† The dynamic characteristics of the filter were investigated and the results are presented in the appendix.

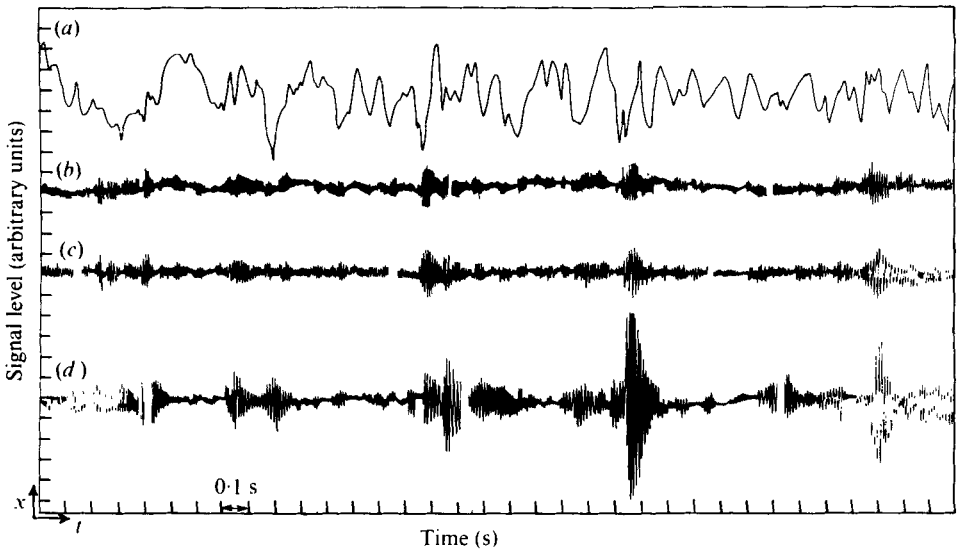

FIGURE 3. Comparison of the sensitivity to bursting of band-pass-filtered u, $\delta u/\delta t$ and $\delta u/\delta r$ signals from a probe in configuration 1. Each trace has about the same level during quiescent periods. $Re_c = 15600$, $y_2^+ = 8{\cdot}41$ and u_2 is the velocity trace from sensor 2. (*a*) u_2. (*b*) u_2, $f_c = 135$ Hz. (*c*) $\partial u_2/\partial t$, $f_c = 135$ Hz. (*d*) $\partial u/\partial r$, $f_c = 135$ Hz.

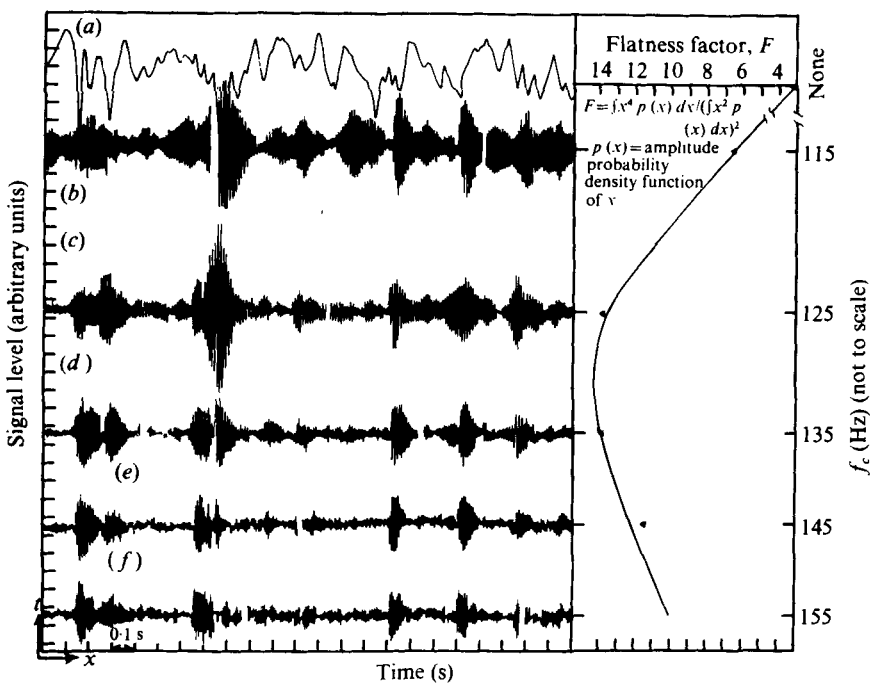

FIGURE 4. Effect of filter frequency on the trace and flatness of a filtered $\delta u/\delta r$ signal. Conditions as in figure 3. The flatness factor is a measure of the size of the bursts relative to the total variance. (*a*) u_2, no filtering. (*b*)–(*f*) $\partial u/\partial r$. (*b*) $f_c = 115$, $F = 6{\cdot}53$. (*c*) $f_c = 125$, $F = 13{\cdot}89$. (*d*) $f_c = 135$, $F = 13{\cdot}89$. (*e*) $f_c = 145$, $F = 11{\cdot}56$. (*f*) $f_c = 155$, $F = 10{\cdot}86$.

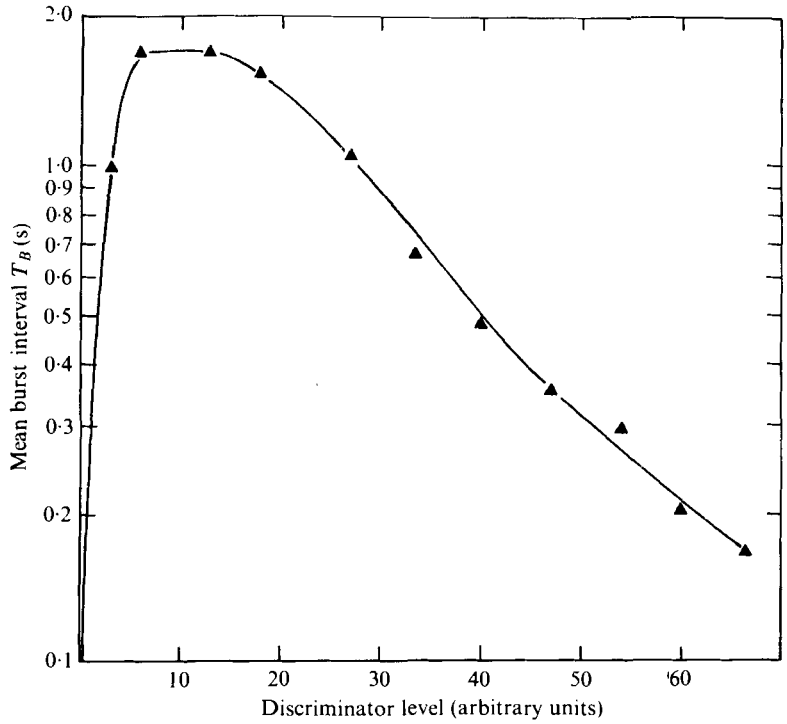

FIGURE 5. Effect of the arbitrary amplitude level set to discriminate 'on' from 'off' on the mean burst interval (f_c = 135 Hz). The burst interval is independent of the discriminator level for settings between about 8 and 16.

level then a burst occurrence is counted. Figure 5 shows that using the same counting procedure as Rao *et al.* a range of discriminator levels exists where the mean burst interval (the reciprocal of the mean burst rate) is independent of the discriminator level.

In general the filter was set at the optimum and, using a discriminator level in the 'independent' range, the number of bursts was counted. The real time length of the signals was varied so that at least 100 bursts were counted for each test. The mean burst rate N was the number of bursts divided by the real time length. (The mean burst interval is $\overline{T}_B = 1/N$.)

4. Results and discussion

4.1. *The relationship between our bursts and those observed by visual techniques*

To determine whether our 'bursts' are the same as those observed by others, we shall first consider the temporal behaviour of the velocity during a measured burst interval as this appears to be at least as important a test as comparing mean burst rates.

Hot-wire anemometer measurements of Lu & Willmarth (1973) have led them to conclude that when the fluctuating velocity is decreasing and becomes sufficiently low a burst will occur which results in large contributions to the Reynolds stress and production of turbulent energy. It has also been observed visually by Corino &

Brodkey (1969) and Kim *et al.* (1968) that a relative minimum in the velocity is followed by an acceleration at the beginning of each active period. We found that this general behaviour was evident when our simultaneous burst signature and velocity traces were compared.

For example, the beginning of the largest burst shown in figure 3(*d*) is accompanied by a relative minimum in the velocity trace (figure 3*a*). A rapid increase in velocity then follows. The velocity behaves in a similar manner during each of the bursts shown in figures 3, 4, 11 and 12. We therefore appear to have identified, at least qualitatively, the same phenomenon as that seen by others in visual studies.

4.2. *Discussion of autocorrelation methods for determining burst rates*

In their study, Kim *et al.* found a weak peak in autocorrelations of the axial velocity fluctuations. The peaks were low and disappeared if the averaging time was long. When detectable, they occurred at a time delay equal to the mean burst interval observed visually. We examined our data to determine whether similar peaks existed in our autocorrelations.

Figure 6 shows several autocorrelations from our data at various Reynolds numbers. The overall behaviour of the correlations is similar. Each correlation drops to zero and then rises at large time delays to a small second peak. The time delay to this peak does *not* correspond to the mean burst interval determined by our technique except in the first case. There is always, however, a small relative maximum in each correlation at a time delay which does equal our mean burst interval. The correlation rise is small and without prior knowledge of where to look it could go unnoticed. Thus we do see the same behaviour in our autocorrelations as did Kim *et al.*

These correlation peaks which may be due to bursts are weak probably because of the time-averaging effects noted by Kim *et al.* (1971) and the relatively large macroscale of our system. Autocorrelations may still be high at time delays larger than the mean burst interval in systems that have a large Eulerian macroscale. Thus a small correlation rise due to bursts may be buried in a region of time delay where the autocorrelation is large. As we approach the wall, the autocorrelations fall off more rapidly and the peak becomes somewhat clearer (see figure 6*b*).

While our data do show weak peaks in the autocorrelations which correspond to mean burst intervals as observed by Kim *et al.*, we feel that this method is not good enough, at least in systems similar to ours, to be used as a burst-rate measurement technique. None of our data are based on this technique.

4.3. *Mean burst rates*

The mean burst rates obtained by our technique are shown in figure 7 for three Reynolds numbers and various values of y^+. The mean burst rate appears to reach a nearly constant value for $y^+ > 30$. The active fluid can strike the probe at any step in the evolution of the burst. Consequently each burst cannot be followed from the beginning. The same difficulty arises with visual observations over localized areas. Thus the measured burst rate is due not only to locally produced bursts but also to those formed elsewhere and convected to the measuring point. The mean time between bursts, which corresponds to the almost constant value attained at the high y^+ values, is therefore more representative of the visual measurements. For a

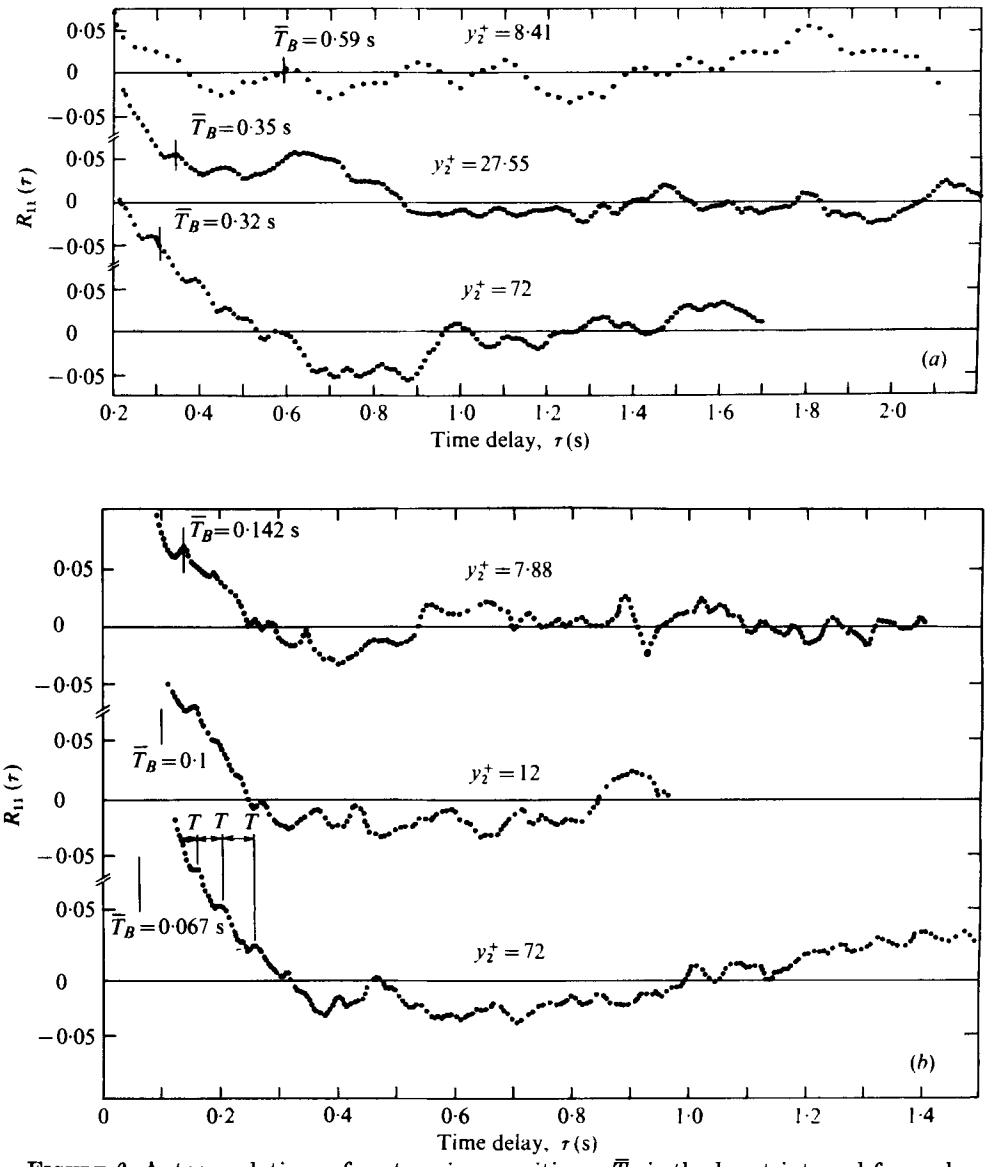

FIGURE 6. Autocorrelations of u at various positions; $\overline{T}_B$ is the burst interval for each position from figure 10. T is the period of the weak oscillation in the correlation curve ($\sim$ 0·067 s). (*a*) Re_c = 15600. (*b*) Re_c = 33000.

Reynolds number of 33000† we used three different probe configurations to obtain mean burst rates. The mean burst rates were found to be independent of the sensor configuration, which tends to build confidence in the whole technique and the data.

Mean burst rates for $y^+ > 30$ are compared with measurements made by others (mainly by visual techniques) in figure 8. Some of the data shown in figure 8 were taken in zero-pressure-gradient boundary layers. In comparing these with the data

† Based on the pipe centre-line velocity and radius.

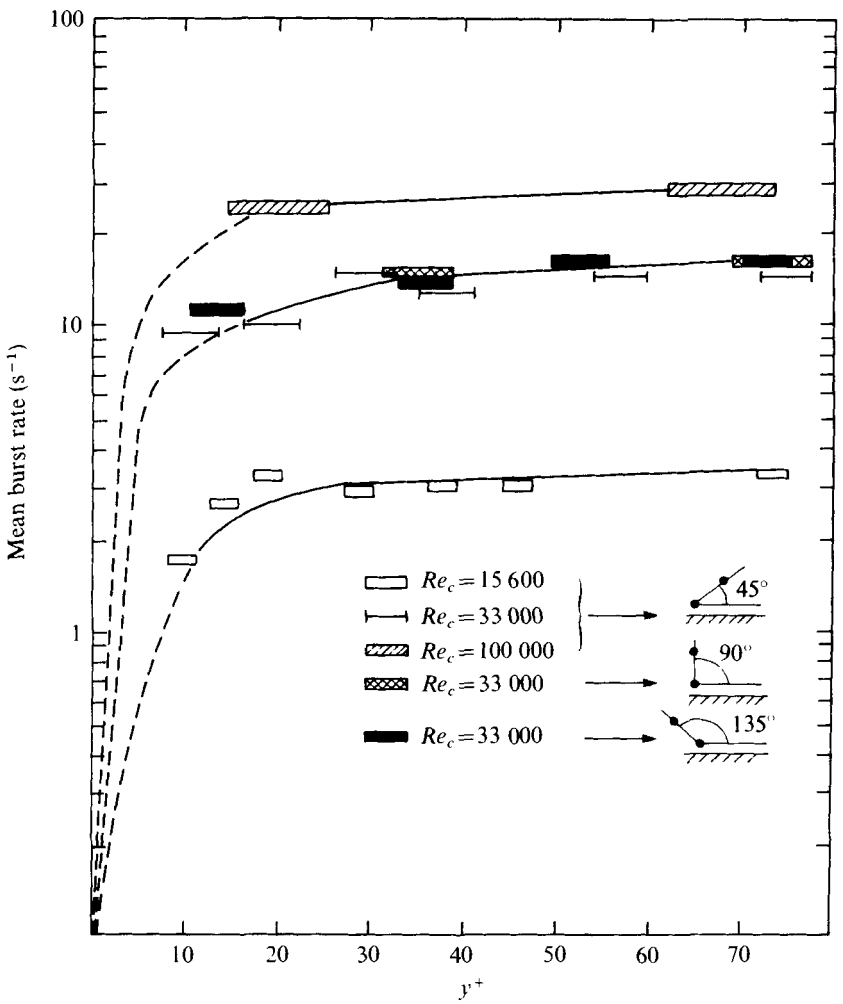

FIGURE 7. Mean burst rate at various positions in fully developed pipe flow. The lateral extent of each point represents the radial separation of the sensors. The agreement of the results when Re_c = 33 000 with three different sensor orientations indicates that the measurements are independent of the probe configuration.

taken in pipes there may be some concern over the effect of the pressure gradient on the burst rate. However, Kline *et al.* (1967) have shown that this effect will be negligible if a parameter related to the pressure gradient, $K = (\nu/U_\infty^3)\,(dP/dx)$, is between 0 and 0·07. In this expression ν is the kinematic viscosity, U_∞ is the free-stream (centre-line in this case) velocity and dP/dx is the pressure gradient. All the data we have shown in figure 8 lie in this range of values of K.

When the friction velocity $U_* = \mu[\partial u/\partial y]_{y=0}$ is less than 4 cm/s the burst intervals are scaled well by U_*^2 (figure 8). For $U_* > 4$ cm/s the data shown are consistent but the scaling and shape of the curve are more questionable. This region will now be discussed in more detail. One point in this region was determined by us from the second peak in Bakewell's (1966) autocorrelation data. The method appears to be

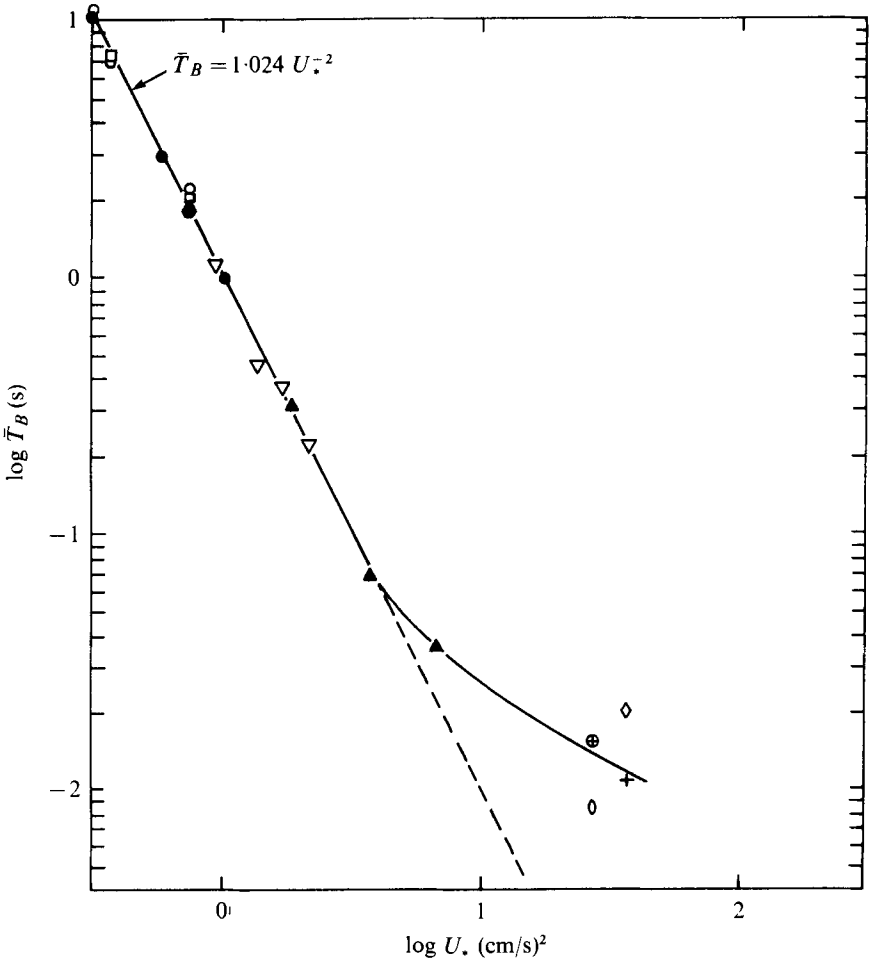

FIGURE 8. Comparison of the burst-rate data from various investigations. ○, Kim *et al.* (1971), visual results in a water boundary layer (b.l.); □, Kim *et al.* (1971), autocorrelation results in a water b.l.; ◖, Schraub & Kline (1965), visual results in a water b.l.; ●, Kline *et al.* (1967), visual results in a water b.l.; ⊕, Rao *et al.* (1971), 'simple' counting in an air b.l. (cf. §2); 0, Rao *et al.* (1971), 'optimum' counting in an air b.l.; ▽, Corino & Brodkey (1969), visual results in trichloroethylene pipe flow; +, Bakewell (1966), autocorrelation in glycerine pipe flow ($y^+ = 10$); ▲, present study, burst signature in water pipe flow.

unreliable as discussed previously. The data of Rao *et al.* are also uncertain. They were determined by their 'simple' procedure, which gave $\overline{T}_B$ values a factor of 2 higher than the 'optimum' procedure described in their paper. Although they used 'simple' values of $\overline{T}_B$ as a basis for comparison with other studies, the 'optimum' values may actually be a better basis and are also shown in figure 8. Owing to limitations in our own experimental facility, results for U_* values greater than 6·71 cm/s could not be obtained. Because of these uncertainties more experiments are necessary before a conclusion can be drawn.

Figure 8 indicates a similarity between the mean burst rate in the constant-stress layer (at low values of U_*) and the turbulent shear stress $\overline{uv}$ since both are correlated

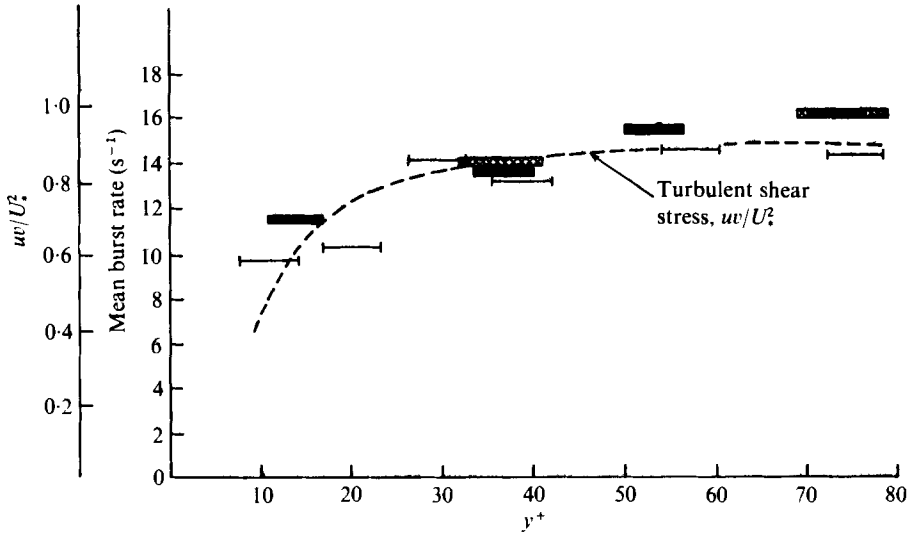

FIGURE 9. Comparison of our experimental burst rates (Re_c = 33000) with the turbulent shear-stress curve of Laufer (1954) ($Re_c \sim$ 33000). The symbols for our data points are the same as in figure 7.

by U_*^2. As shown in figure 9, the mean burst rate and $\overline{uv}$ also vary similarly with y^+ in the region where data are available.

$\overline{T}_B$ does not appear to be a function of the inner variables U_*^2 and ν alone. If it were, then the values of $U_*^2/\nu N$ for trichloroethylene and water would be the same; which is not the case. In fact, in figure 10 we show that N is virtually independent of one of these inner variables, ν, since the data appear to be better correlated by removing the viscosity from the abscissa. No non-dimensional group could be found which adequately scaled all the results.

4.4. *The internal characteristics of bursts*

Figure 11 shows two sets of simultaneous values of u_1 (i.e. the velocity measured with sensor 1 of figure 1), $\partial u_1/\partial t$, $\partial u/\partial r$ and the envelope formed by the frequency component of our method of burst identification, for the conditions indicated. This envelope is formed by joining the peaks of the sine-wave output of our filter with two smooth curves. During the bursts shown the behaviour of the velocity during active intervals in the burst envelope can be seen to be similar to the behaviour observed during bursting in visual studies.

The beginning of an active period in the burst envelope is always accompanied by a positive spike in $\partial u/\partial t$. This is a necessary, rather than a sufficient, condition since a burst does not follow all peaks in $\partial u/\partial t$. The time when $u(t)$ is at a relative minimum just before this spike is a convenient time to define as the beginning of a burst. Near the end of each active interval there is always a time when $\partial u/\partial t = 0$, which we defined as its end. If the motion of the disturbance was pure translation the period between the beginning and end would be related to its size in space.

The behaviour of several variables within three typical bursts is shown in figure 12. The bursts are those starting at 3·965, 4·125 and 5·245 s in figure 11. The values of

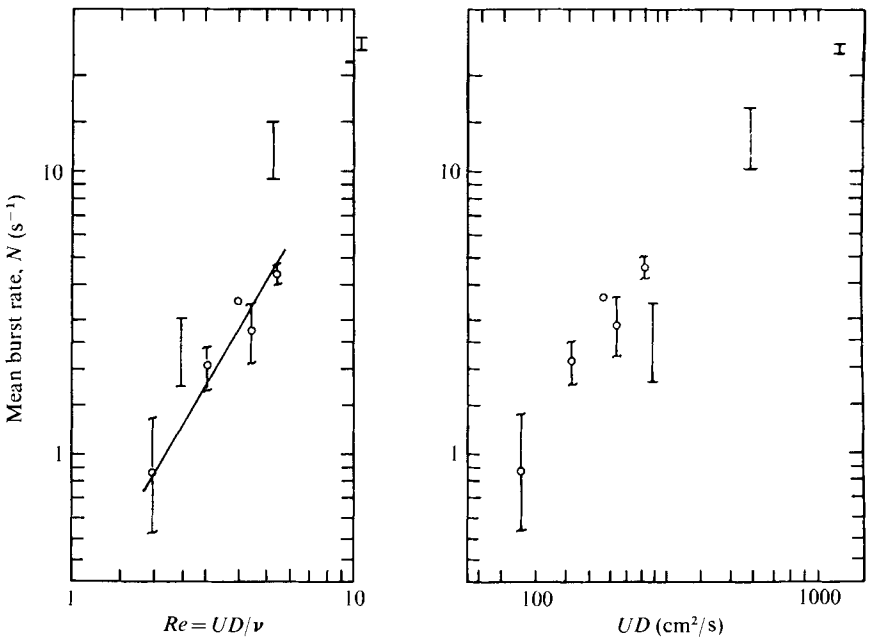

FIGURE 10. Comparison of the burst rates of two different fluids in fully developed pipe flow. Φ, data of Corino & Brodkey (1969) in trichloroethylene (ν = 0·419 cS); I, data of the present study in water (ν = 1·022 cS). The diameter D of the pipe used by Corino & Brodkey was 5·08 cm, our D was 7·87 cm. Bars on our points indicate the range of variation in the burst rate due to y^+ (as shown on figure 9). U is the average velocity in the pipe.

each of the variables at the beginning of the burst have been subtracted, since these represent the conditions measured in the flow just before the 'active' fluid strikes the probe. The measurements were all made with probe configuration 1 (see figure 1). The spatial derivative $\partial u/\partial r$ obtained from this probe is inclined at 45° to the flow axis. The cross-stream spatial derivative $\partial u/\partial y$ is also plotted in figure 12. It was calculated from $\partial u/\partial r$ and $\partial u/\partial t$ by assuming a frozen flow pattern.

Each burst began with a relative minimum in the axial velocity followed by simultaneous peaks in $\partial u/\partial r$, $\partial u/\partial t$ and $\partial u/\partial y$. About half-way through the burst $\partial u/\partial r$ and $\partial u/\partial y$ peak again, shortly after a second relative minimum in the axial velocity trace. This behaviour occurred for all the bursts we have examined. It appears to be somewhat similar to the sequence of events in the last stage of laminar-to-turbulent transition observed by Kovasznay, Komoda & Vasudeva (1962). Measurements of the cross-stream velocities (v and w) and their derivatives within bursts are necessary before conclusions can be drawn.

Short-term energy spectra of u during each burst were obtained and typical results are shown in figure 13. The peaks in the energy spectra taken within bursts agree with the weak periodicity observed in the velocity traces of figure 11. Although most burst spectra had peaks, the frequency of these peaks 'jittered' from burst to burst. Thus conventional ensemble averaging of the energy spectra of many bursts produced the smooth curve also shown on figure 13. Since any short-time-averaged spectrum may have a peak in it somewhere (depending on the averaging time), it will be necessary to perform some sort of conditional averaging of many spectra before a definite

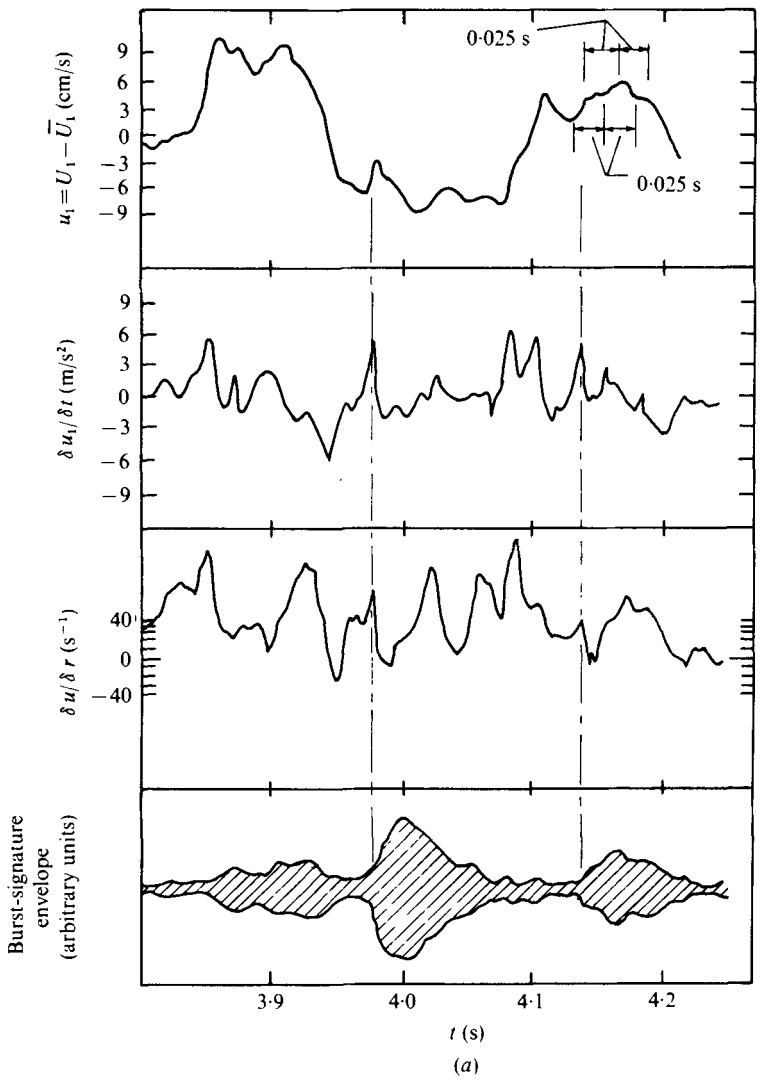

(a)

FIGURE 11(a). For legend see next page.

periodicity can be identified. However, a 'jitter' in wavelength is consistent with a two-part model (Lahey & Kline 1971) which has successfully represented some of the structural features of turbulent boundary layers. This model hypothesizes the interaction of organized disturbance waves with background turbulence. Our measurements both here and in part 1 support the use of this type of two-part model to describe turbulent wall layers rather than an 'average eddy' structure.

5. Conclusions

Filtered cross-stream spatial derivatives of the axial velocity have intermittent periods of activity which appear to correspond to visually observed bursts. These spatial derivatives are more sensitive to bursts than either the velocity or the

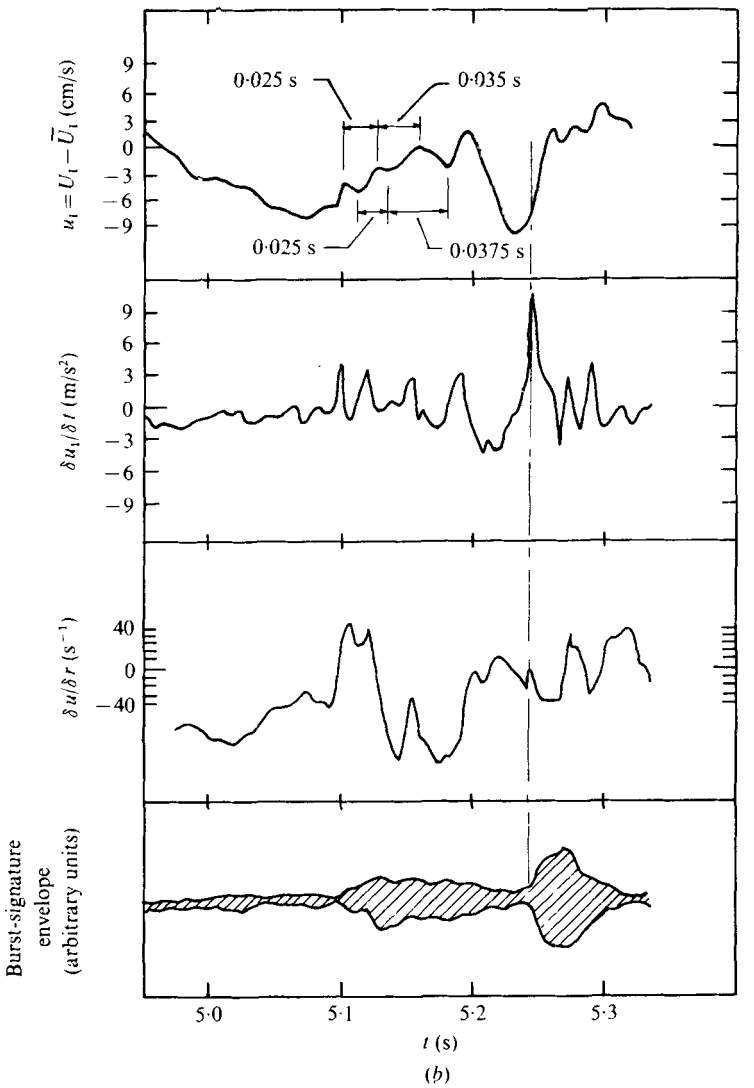

FIGURE 11. (*a*) Typical simultaneous velocities and time and space velocity derivatives and the burst envelope from a probe in configuration 1. $Re_c = 15600$, $y_2^+ = 12{\cdot}96$. (*b*) Same as (*a*) but over a different time interval.

filtered velocity time derivative signals that have been used by previous investigators.

For $U_* < 4$ cm/s the mean burst rate N and the turbulent shear stress $\overline{uv}$ are similar since both are correlated by U_*^2 in the constant-stress layer. N and $\overline{uv}$ also vary similarly with y^+ (in this range of U_*). Sufficiently good data for $U_* > 4$ cm/s are not available.

We have shown that N cannot be reliably determined solely from long-time-averaged autocorrelation measurements of u. This is partly because the small correlation rise due to bursts may be buried in a region where the time correlation is

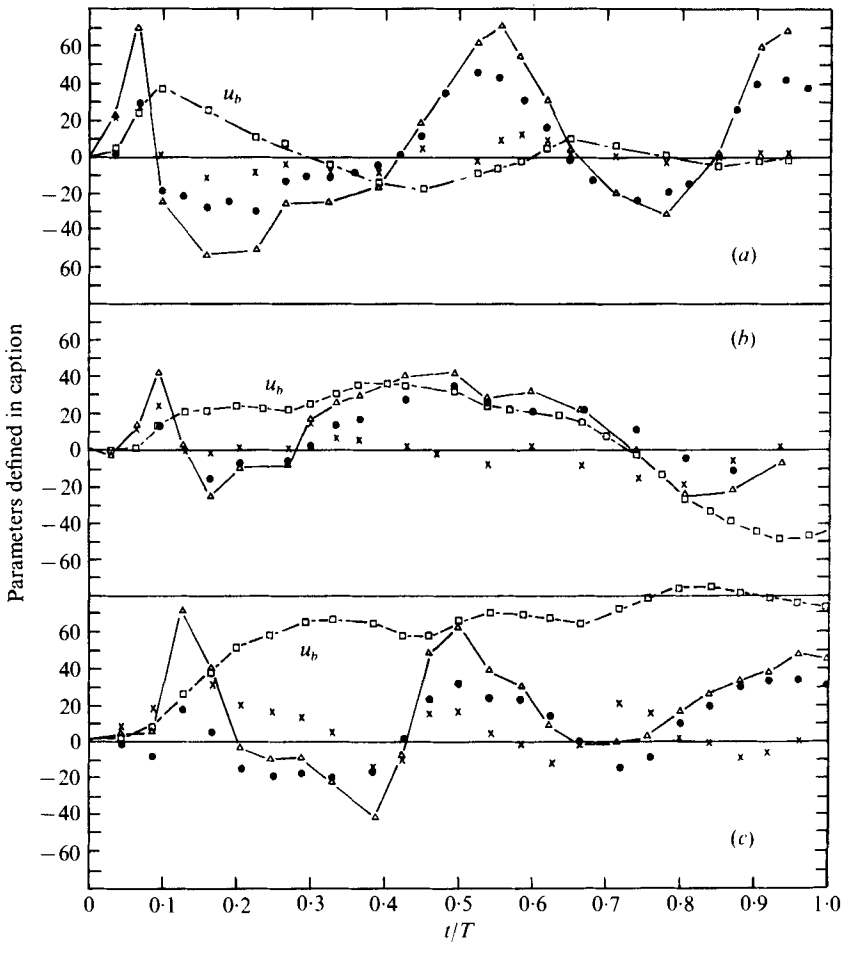

FIGURE 12. Behaviour of several variables within typical burst intervals (see figure 11). (*a*) Burst at 3·96 s. (*b*) Burst at 4·12 s. (*c*) Burst at 5·24 s. □, $\dfrac{C-(u(t/T)-u(0))}{\bar{U}T} = u_b$, where C = arbitrary scaling factor, T = duration of burst and t = elapsed time from beginning of burst;

$$\bullet,\ \frac{\partial u}{\partial r}\bigg|_{t/T} - \frac{\partial u}{\partial r}\bigg|_0 = \left(\frac{\partial u}{\partial r}\right)_b;\ \times,\ \frac{\partial u}{\partial t}\bigg|_{t/T} - \frac{\partial u}{\partial t}\bigg|_0 = \left(\frac{\partial u}{\partial t}\right)_b;\ \triangle,\ 2\tfrac{1}{2}\left(\frac{\partial u}{\partial r}\right)_b + \frac{1}{U}\left(\frac{\partial u}{\partial t}\right)_b = \left(\frac{\partial u}{\partial y}\right)_b.$$

large. Thus any previous determinations of N that used long-time-averaged autocorrelations should be treated with caution.

Bursts begin with a local velocity minimum followed by simultaneous relative maxima in $\partial u/\partial t$ and the spatial derivatives $\partial u/\partial r$ and $\partial u/\partial y$. A second velocity minimum and second maxima in the spatial derivatives occur about half-way thrpugh the burst. The second peaks are about the same height as the first. This sequence occurs for all the bursts analysed. Also, the velocity during bursts exhibits a weak periodicity which causes a peak in energy spectra taken during burst intervals. The overall behaviour has some of the features observed in the last stage of laminar-to-turbulent flow transition.

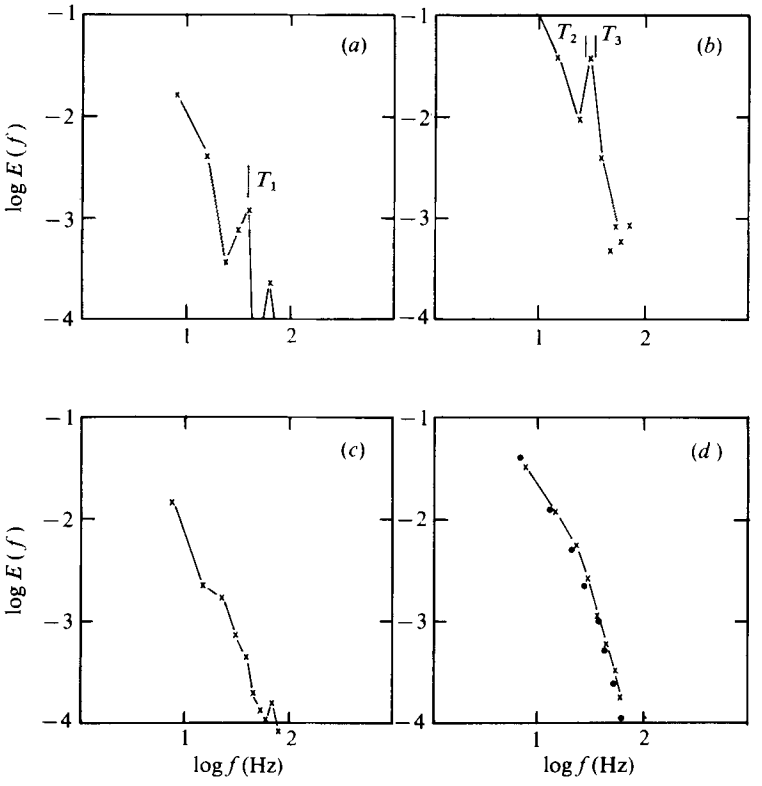

FIGURE 13. Typical energy spectra $E(f)$ of $u(t)$ taken during the active and passive intervals shown on figure 11. (*a*) Burst interval from 4·13 to 4·2 s. (*b*) Burst interval from 5·1 to 5·22 s. (*c*) Quiet interval from 4·85 to 5·1 s. (*d*) X-ensemble average of 15 bursts; ●, 1 min time average. All spectra are normalized by the 1 min average variance. The time intervals shown correspond to the intervals indicated on figure 11. $T_1 = 0{\cdot}025$ s, $T_2 = 0{\cdot}0375$ s, $T_3 = 0{\cdot}0325$ s.

This work was done at the Whiteshell Nuclear Research Establishment of Atomic Energy of Canada Limited with financial support for one of the authors (T.R.H.) provided by both the National Research Council and Manitoba Hydro.

Appendix. Filter characteristics

A Bruel & Kjaer spectrum analyser was used to produce the 'burst signatures' presented in this paper. Hence the filter characteristics, both average and dynamic, were investigated.

The average pass band of the filter was determined experimentally and was found to be 6 % of the filter centre-frequency. The dynamic characteristics of the filter were investigated by putting both intermittent sine-wave bursts and a series of ramp voltage changes into the spectrum analyser. The centre-frequencies of the analyser in these tests were set to the same values as were used to obtain the burst results of §3.3.

The filter consistently took ~ 15 periods of its centre-frequency fully to respond to the step input and ~ 20 periods totally to decay. Thus we were certainly able to

sense input events that had at least a 15 cycle duration and occurred at least 36 cycles apart. In actual fact, we could sense events that happenned much more frequently since the filter is not required either to attain an equilibrium value or to decay fully to zero. Results discussed in detail in Heidrick (1974) show that the filter's response was sufficiently rapid to detect input burst rates in excess of the measured burst rates of §3.3. Hence, if these results may be extended to input events of the type sensed in §3.3, it may be concluded that the filter did not impose a false limit on the number of bursts sensed. The fact that the number of bursts on the output traces of § 3.3 were independent of the filter centre-frequency over a certain range of frequencies (figure 4) also supports this conclusion. If the filter was imposing a limit on the number of bursts, the burst rate would continue to increase with increasing centre-frequency.

Heidrick (1974) also shows that there was no time displacement between a change in the input to the analyser and the beginning of the change in the output from the analyser. Thus the beginning of an input burst could be accurately determined from the output trace. The reaction to the input wave going off was also immediate. However, for a less regular input pattern it might be difficult to determine the end of an input burst from the output trace.

When a filter is subjected to a sudden change in voltage it will 'ring' and produce a signal for a finite time after the change. Hence this property of the filter was investigated by subjecting the filter to a variety of ramp inputs.

The amount of filter ringing caused by several different speeds of ramp voltage input is given by Heidrick (1974). The length of time the filter rang was inversely proportional to the filter centre-frequency. For a given ramp input speed, the amplitude of the ringing was essentially constant over a range of filter centre-frequencies. This frequency range, however, was different for different input ramp speeds. This indicates that the amplitude of the ringing is dependent on both the filter setting and the rise time of the input pulse. When the filter centre-frequency was very high the ringing disappeared for each type of input. The faster the input rise time the higher the frequency had to be to cause the ringing to disappear.

The behaviour described above was also observed for ramp decreases in voltage and gives a possible explanation for the behaviour of the flatness factor observed in §3. For a series of fixed speed and size ramp inputs the flatness factor would remain constant over the range of frequencies where the ringing amplitude was independent of the filter centre-frequency. If the centre-frequency was further increased both the height of the ringing pulses and the flatness factor would also decrease. This type of behaviour would also be expected for a series of voltage changes of various sizes and speeds, such as those of the input signal described in §3. The average size of the pulses in the output, and hence the flatness factor, would start to decrease when the filter setting was raised past a certain setting f'. The value of f' would depend on both the amplitudes and the speeds of the voltage changes in the input signal. At filter settings higher than f' the pulses, on the average, would begin to decrease in size and the inherent noise in the filter output signal would become a larger proportion of the total output. Thus the decreasing flatness factor described in §3 is probably due to a combination of filter characteristics, and the size and shape of the pulses in the input signal.

REFERENCES

BAKEWELL, H. P. 1966 Ph.D. dissertation, The Pennsylvania State University.

CORINO, R. E. & BRODKEY, R. S. 1969 *J. Fluid Mech.* **37**, 1.

HEDLEY, T. B. & KEFFER, J. F. 1974 *J. Fluid Mech.* **64**, 625.

HEIDRICK, T. R. 1974 Ph.D. dissertation, The University of Manitoba.

HEIDRICK, T. R., BANERJEE, S. & AZAD, R. S. 1977 *J. Fluid Mech.* **81**, 137.

KAPLAN, R. E. & LAUFER, J. 1969 *Proc. 12th Int. Cong. Appl. Mech.* Springer.

KIM, H. T., KLINE, S. J. & REYNOLDS, W. C. 1968 *Thermosci. Div., Dept. Mech. Engng, Stanford Univ. Rep.* MD-20.

KIM, H. T., KLINE, S. J. & REYNOLDS, W. C. 1971 *J. Fluid Mech.* **50**, 133.

KLINE, S. J., REYNOLDS, W. C., SCHRAUB, F. A. & RUNSTADLER, P. W. 1967 *J. Fluid Mech.* **30**, 741.

KOVASZNAY, L. S. G., KOMODA, H. & VASUDEVA, B. R. 1962 *Proc. Heat Transfer Fluid Mech. Inst.* p. 1. Stanford University Press.

LAHEY, R. T. & KLINE, S. J. 1971 *Thermosci. Div., Dept. Mech. Engng, Stanford Univ. Rep.* MD-26.

LAUFER, J. 1954 *N.A.C.A. Rep.* no. 1174.

LU, S. S. & WILLMARTH, W. W. 1973 *J. Fluid Mech.* **60**, 481.

OFFEN, G. R. & KLINE, S. J. 1975 In *Turbulence in Liquids* (ed. J. L. Zakin & G. K. Patterson), p. 289. University of Missouri Rolla Press.

RAO, K. N., NARASIMHA, R. & BADRI NARAYANAN, M.A. 1971 *J. Fluid Mech.* **48**, 339.

RICHARDSON, F. M. & BEATTY, K. O. 1959 *Phys. Fluids* **2**, 718.

SALTVOLD, J. S. 1971 *Proc. DECUS (Digital Equipment Users Soc.) Symp., Fredericton, New Brunswick.*

SCHRAUB, F. A. & KLINE, S. J. 1965 *Thermosci. Div., Dept. Mech. Engng, Stanford Univ. Rep.* MD-12.

WALLACE, J. M., ECKELMANN, H. & BRODKEY, R. S. 1972 *J. Fluid Mech.* **54**, 39.